Planet. Space Sci., Vol. 40, No. 9, pp. 1237–1250, 1992
Printed in Great Britain.

0032-0633/92 $5.00 + 0.00

A MODEL FOR THE ENERGY BUDGET OF THE ATMOSPHERE: COMPARISON WITH DATA FROM THE EARTH RADIATION BUDGET EXPERIMENT

KENNETH MINSCHWANER and MICHAEL B. McELROY
Department of Earth and Planetary Sciences and Division of Applied Sciences,
Harvard University, Cambridge, MA 01238, U.S.A.

(*Received* 13 *March* 1992)

Abstract—A radiative–convective model is developed and used to examine the sensitivity of clear-sky fluxes of infrared radiation to changes in sea surface temperature, atmospheric lapse rates and relative humidity. The radiative model uses the correlated-k method and includes an improved treatment of the finite-difference approximation in the evaluation of the vertical flux integral. Absorption coefficients are calculated directly from spectroscopic data. Model results for radiative cooling rates agree with benchmark line-by-line calculations to better than 5%.

Comparison with ERBE (Earth Radiation Budget Experiment) measurements indicates that a 6.5 K km^{-1} lapse rate model would be inconsistent with infrared fluxes observed at the top of the atmosphere. Agreement is improved significantly using a parameterization in which the static stability is specified empirically as a function of surface temperature. A model with a latitudinally fixed profile for relative humidity as a function of pressure is consistent with the observational data for surface temperatures less than about 298 K. Comparison with measurements for higher temperatures suggests that significant increases in middle and upper tropospheric humidity may be associated with warmer sea surface temperatures. The enhanced greenhouse forcing at high surface temperatures is felt primarily in the atmosphere, rather than at the surface. Implications of the clear-sky radiative deficit inferred for the atmosphere in the tropics are discussed.

1. INTRODUCTION

The composition of the atmosphere is changing at an impressive rate at the current time, due largely to the effects of human activity. A major contemporary challenge is to predict the effects of changes in atmospheric composition on climate. The response of the climate system to variations in the abundances of CO_2, CH_4, N_2O, O_3 and CFCs implies a series of complex interactions. Feedbacks involving water are of particular significance. The evaporation–condensation cycle provides an important, often dominant, means for transfer of energy from the surface to the atmosphere, and from one region to another. Water in vapor form is the most important greenhouse agent, regulating to a large extent the transfer of infrared energy between the surface and the atmosphere and between the atmosphere and space. Water in the condensed phase plays a dual role: clouds affect the albedo of the Earth, limiting the flux of visible solar radiation penetrating to the surface; they also constitute an important component of the atmospheric greenhouse. Given the central importance of water for the climate system, a minimum requirement for models is that they provide a realistic simulation of the physical processes affecting the abundance and distribution of H_2O.

It is clear that further work is required to meet this goal. A key question concerns the mechanism for vertical transport of water. There have been suggestions that an increase in CO_2 and other greenhouse gases could, by stimulating enhanced convective activity in the tropics, result in a reduction in the abundance of water vapor in the upper troposphere (Ellsaesser, 1984; Lindzen, 1990). This argument is based on the assumption that the water vapor content of the upper troposphere is determined primarily by the temperature at which air is detrained from the tops of cumulus clouds. Warming at the surface could result in higher, and thus colder, detrainment levels; in this case, one might expect air detrained from the tops of cumulus towers to be drier. On the other hand, there is reason to believe that the water vapor content of the upper troposphere is controlled not simply by detrainment of water in the gas phase, but also by detrainment and subsequent evaporation of H_2O transported to upper levels of the troposphere in the form of either ice or liquid. The importance, and even the sign, of the feedback is unclear. It is unlikely that the dilemma will be resolved by contemporary models emphasizing first principles. The scales of motion relevant for convective systems are too small to be resolved by even the highest resolution general circulation models of the atmosphere.

A more empirical approach is adopted here. We describe a model in which rates of radiative cooling

and fluxes of infrared radiation are computed with high precision, with lapse rates for temperature specified as a function of surface temperature on the basis of observational data (Rennick, 1977). The model is applied to analysis of results from the Earth Radiation Budget Experiment (ERBE) (Barkstrom, 1984), specifically to data for the cloud-free atmosphere. The approach is complementary to that used by Raval and Ramanathan (1989). They focused on the difference between the flux of infrared radiation emitted by the surface and the flux emitted to space, identifying this quantity as the available greenhouse radiation. A more conventional definition would associate the greenhouse radiation with the flux of infrared radiation from the atmosphere to the surface. A conceptual summary of the different contributions to the energy budget of a column of clear atmosphere is presented in Fig. 1. We have chosen here to focus separately on $F\uparrow_T$, the radiant energy emitted to space; on $F\downarrow_S$, the flux of infrared radiation returned to the surface by the atmosphere; and on S, the height integrated rate for absorption of solar radiation by the atmosphere. We are able in this case, by adjusting our model to agree with ERBE data for the flux of radiation emitted to space ($F\uparrow_T$), to estimate as a function of surface temperature the magnitude of the non-radiative contribution to the energy budget of the clear atmosphere.

The model is described in Section 2. Structurally, it is similar to radiative–convective models developed and employed extensively over the past few decades

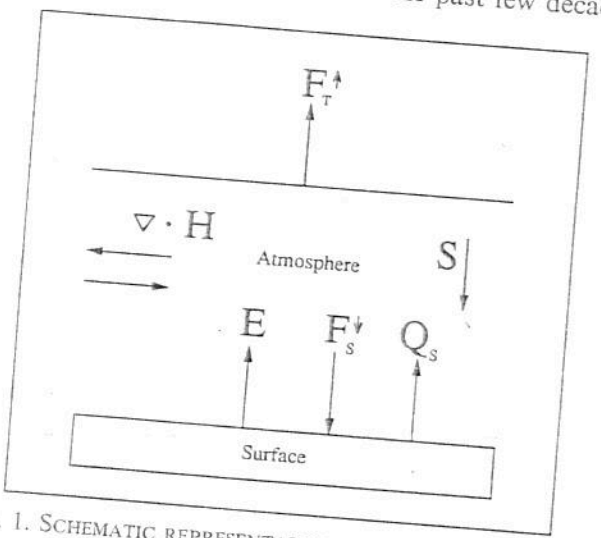

FIG. 1. SCHEMATIC REPRESENTATION OF THE ENERGY BUDGET FOR A COLUMN OF CLEAR ATMOSPHERE.
$F\uparrow_T$ defines the emergent infrared flux at the top of the atmosphere; $F\downarrow_S$ is the downward infrared flux incident at the surface; E is the upward flux emitted by the surface; S is the solar energy absorbed in the atmosphere; Q_S is the flux of sensible heat from the surface to the atmosphere; and $\nabla \cdot H$ is the divergence of the horizontal flux of dry static energy.

to study the globally averaged impact of changes in atmospheric composition, the a doubling in CO_2 for example (Mana Wetherald, 1967; Ramanathan, 1976; Hanse 1981; Vardavas and Carver, 1984). Factor encing the flux of radiation emitted to space cussed in Section 3. It is shown than a model fixed profile for relative humidity provides ex agreement with the ERBE data when the surfac perature is less than about 298 K. Emergent obtained with the model are larger than ob values for higher temperatures. The behavior fo face temperatures in excess of 298 K is related super-greenhouse phenomenon noted by Rava Ramanathan (1989). The high temperature and is attributed here to an increase in the re humidity of the troposphere at pressure levels b about 500 mbar. The trend inferred for water v suggests that elevated surface temperatures are as ated with an enhanced supply of H_2O to the u troposphere. Implications for the back-radiation to surface and the net radiative forcing of the atmospl as a function of surface temperature are discussed Section 4. Conclusions are summarized in Section

2. RADIATIVE–CONVECTIVE MODEL

Transfer of energy by infrared radiation in t Earth's atmosphere involves absorption and emissio of light over a broad region of the spectrum. A varie of constituents are implicated, with radically differen density profiles and a wide range of absorptio efficiencies. A detailed, spectrally resolved, simulatio of energy transfer would require treatment of radi ation on a line-by-line basis. Such a calculation could be implemented in a straightforward manner given sufficient computing power and adequate information on relevant absorption coefficients. Computation of infrared fluxes using a line-by-line approach would represent, however a formidable task. Individual integration steps require evaluation of complex functions, exponential integrals and Voigt line profiles, for example. Depending on the choice of spectral and altitude resolution, the number of computational steps required to evaluate the infrared radiation field for a specified model atmosphere may exceed 10^9. Use of a line-by-line approach for climate models, even for the simple case of one-dimensional radiative equilibrium, is impractical; the computational burden is simply too severe.

A variety of schemes have been devised to address this problem. They often involve approximations in which a complex molecular band is replaced by a single effective spectral line, with parameters chosen

to simulate the mean transmission of radiation in the band. In other cases, emission and absorption of infrared radiation by an inhomogeneous slab of atmosphere is represented in terms of an effective emissivity, with scaling arguments used to define appropriate mean values for pressure and temperature [see Goody and Yung (1989) for a complete discussion]. It is difficult to assess the magnitude of errors introduced by approximations in common use for specific applications, but line-by-line results can provide a useful benchmark [Ridgeway *et al.* (1991); Fels *et al.* (1991)]. The Intercomparison of Radiation Codes used in Climate Models (ICRCCM) program concluded that differences in vertical resolution and quadrature schemes were largely responsible for discrepancies in clear-sky fluxes computed with different models (Ellingson *et al.*, 1991). The study emphasized particularly the importance of the integration scheme used to account for contributions to the local flux from neighboring regions. Radiative fluxes obtained with the better approximate schemes agreed with line-by-line calculations to within a few percent, at least for the limited range of model atmospheres investigated by ICRCCM, although errors in some cases were found to exceed 10% (Ellingson *et al.*, 1991).

We developed, for present purposes, an efficient algorithm that allows us to compute infrared heating rates avoiding many of the approximations used in earlier atmospheric models. A statistical approach, termed the correlated-k method in recent applications to the atmosphere (Goody *et al.*, 1989; Lacis and Oinas, 1991), is used to carry out the necessary spectral integrations (Arking and Grossman, 1972; Hansen *et al.*, 1983). This technique has also been used previously to treat absorption in the atmosphere of solar ultraviolet in the Schumann–Runge band system of O_2 (Fang *et al.*, 1974). The advantage of the method is that it can account in a computationally efficient manner for the complex structure of vibration–rotation transitions for all of the molecules of interest in the atmosphere.

Consider an altitude z in a plane parallel atmosphere. The net vertical (upward) flux of infrared radiation for a spectral interval $\Delta\nu$, $F^{\Delta\nu}(z)$, is given by:

$$F^{\Delta\nu}(z) = 2\pi \int_{\nu}^{\nu+\Delta\nu} d\nu \left(B_\nu(T^*)E_3(\tau_\nu^* - \tau_\nu) + \int_{E_3(\tau_\nu - \tau_\nu)}^{0.5} B_\nu[T(t_\nu)]\, dE_3(t_\nu - \tau_\nu) - \int_{E_3(\tau_\nu)}^{0.5} B_\nu[T(t_\nu)]\, dE_3(\tau_\nu - t_\nu) \right). \quad (1)$$

Here, ν = wavenumber; B_ν = the Planck function; T = the temperature of the atmosphere at the altitude characterized by an optical depth t; T^* = the temperature at the ground; τ_ν = the optical depth at level z; τ_ν^* = the optical depth at the ground; $E_3(x)$ = the exponential integral $\equiv \int_1^\infty (e^{-\omega x}/\omega^3\, d\omega)$. The exponential integrals in equation (1) arise as a result of the angular integrations involved in the evaluation of the flux. They are approximated frequently in terms of exponential functions, e^{-rx}, with the exponent r, known as the diffusivity factor, selected to represent a mean angle of propagation for the radiation field ($r = 1/\mu$, where μ is the cosine of the zenith angle), usually set equal to 1.66. This introduces errors in the evaluation of fluxes that can be avoided by implementing an efficient method for direct evaluation of $E_3(x)$. The first two terms in equation (1) account for the upward component of the flux; the third represents the contribution from radiation propagating in the downward direction. The net flux in equation (1) is an implicit function of altitude through the variation of τ_ν with z, defined by:

$$\tau_\nu(z) = \int_z^\infty n(z')k_\nu\, dz', \quad (2)$$

where n is the density of the absorber and k_ν is the absorption coefficient.

The radiative cooling rate, Q_R, may be evaluated in terms of the flux divergence:

$$Q_R = -\frac{1}{\rho c_p}\frac{\partial F}{\partial z}, \quad (3)$$

where ρ is the total mass density and c_p is the specific heat at constant pressure. The difficulty in calculating infrared cooling rates relates to the integration over wavenumber in equation (1). The absorption coefficient can vary by an order of magnitude over a relatively small wavenumber interval. Problems are most severe for the upper stratosphere where line widths are narrow, with Doppler half-widths of about 0.001 cm^{-1}. Line-by-line calculations using a fixed spectral grid require a minimum of four points per line half-width to resolve individual spectral features. A total of 10^6 spectral points would be needed to describe the 9.6 μ band of O_3.

The computational expense can be reduced significantly with a transformation of variables from wavenumber to a cumulative probability function of the absorption coefficient. Based on a statistical analysis of the distribution of k_ν in an interval $\Delta\nu$, we develop first the probability density function, $f(k)$, such that $f(k')\, dk'$ defines the probability of finding a value of k between k' and $k' + dk'$ within the interval

$\Delta\nu$. The integral of a single-valued function of k can be transformed as follows:

$$\int_{\nu}^{\nu+\Delta\nu} y(k_\nu)\,d\nu = \Delta\nu \int_{k_{min}}^{k_{max}} y(k')f(k')\,dk'. \quad (4)$$

A more compact representation of the integral in equation (4) is obtained by a further transformation, introducing the cumulative probability function, $g(k')$, given by:

$$g(k') = \int_0^{k'} f(k)\,dk. \quad (5)$$

The function, $g(k')$, defines the probability of finding a value of k less than k' within the interval $\Delta\nu$. From equation (5):

$$dg = f(k')\,dk' \quad (6)$$

and equation (4) becomes:

$$\int_{\nu}^{\nu+\Delta\nu} y(k_\nu)\,d\nu = \Delta\nu \int_0^1 y(k_g)\,dg. \quad (7)$$

If y is a relatively smooth function of k, e.g. equation (1), then the integrand on the right-hand side of equation (7) varies slowly with respect to the new integration variable, in contrast with the case of the integrand on the left. It follows that the number of quadrature points required to evaluate the integral on the right should be significantly less than for that on the left. The transformation from k_ν to k_g is possible since $g(k)$ is a monotonic function of k. The transformation given by equation (7) permits an ordering of quadrature points in terms of increasing values of k; nearly identical values of k are grouped and weighted according to their frequency of occurrence. Examples of the $\nu \rightarrow g$ transformation for CO_2 are illustrated in Fig. 2(a, b) for representative values of pressure and temperature.

Consider a wavenumber interval in equation (1) for which the Planck function can be replaced by an appropriate mean value. Little error is introduced by replacing B_ν by its average over $\Delta\nu$ for values of $\Delta\nu$ equal to about 50 cm^{-1}. Using the transformation (7), the net flux integrated over the spectral interval $\Delta\nu$ is given by:

$$F^{\Delta\nu}(z) = 2\pi\Delta\nu \int_0^1 dg \left(B^{\Delta\nu}[T^*]E_3(\tau_g^* - \tau_g) + \int_{E_3(\tau_g^* - \tau_g)}^{0.5} B^{\Delta\nu}[T(t_g)]\,dE_3(t_g - \tau_g) - \int_{E_3(\tau_g)}^{0.5} B^{\Delta\nu}[T(t_g)]\,dE_3(\tau_g - t_g) \right) \quad (8)$$

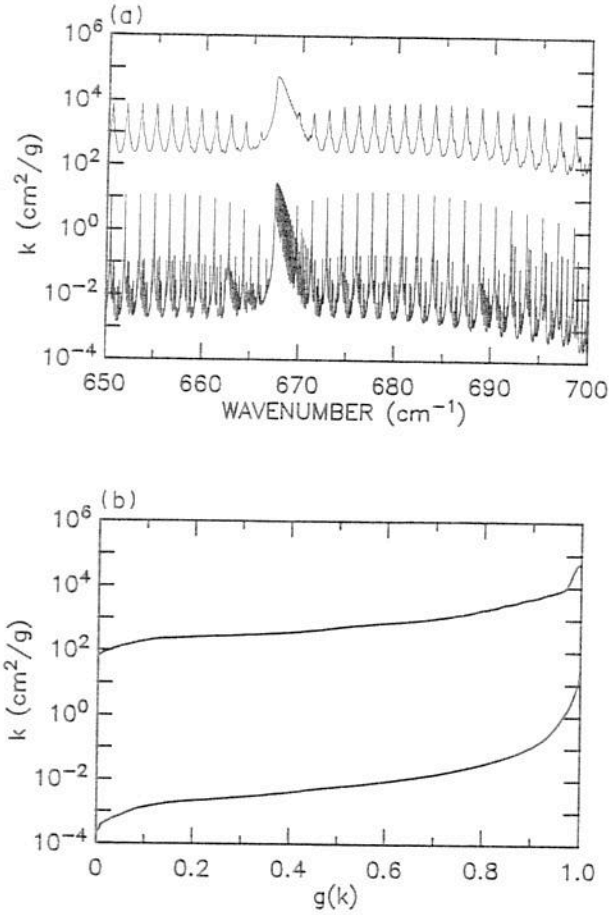

FIG. 2. (a) ABSORPTION COEFFICIENT FOR CO_2 AS A FUNCTION OF WAVENUMBER FOR A TEMPERATURE AND PRESSURE OF 300 K AND 1013 mbar (TOP), AND 209 K AND 52 mbar (BOTTOM). The absorption coefficient for the lower of the two curves was multiplied by a factor of 10^{-4} for ease of presentation. (b) The cumulative distribution function, $g(k)$, for CO_2 in the interval 650–700 cm^{-1} corresponding to the combinations of temperature and pressure in (a). The lower curve has been multiplied by a factor of 10^{-4}.

where:

$$\tau_g(z) = \int_z^\infty n(z')k_g\,dz'.$$

Equation (8) is exact for a homogeneous atmosphere, i.e. the nature of the transformation $\tau_\nu \rightarrow \tau_g$ is the same for all altitudes; the spectral dependence of the absorption coefficient is correlated at all altitudes. In practice, spectral line strengths and widths are expected to vary with altitude in response to changes in pressure and temperature. Studies by Goody *et al.* (1989) and Lacis and Oinas (1991) indicate that errors introduced by the assumption that the spectral dependence of k is correlated for different altitudes are small, typically less than 1%. Effective transmission of infrared radiation is limited, for most spectral intervals, to paths for which changes in pressure and tem-

perature are insufficient to require significant modification to the $\tau_v \rightarrow \tau_g$ transformation.

Our model consists of 40 levels, at 1 km intervals below 20 km and at 2 km intervals above. The vertical grid spacing is decreased near the surface to about 0.5 km. We distinguish between levels (specific altitudes for which values of optical depths and fluxes are calculated), and layers (regions bounded by adjacent levels). Mean absorption coefficients are computed from the outset for individual layers using line parameters included in the AFGL spectral compilation (Rothman *et al.*, 1986), with reference profiles for temperature and pressure taken from McClatchey *et al.* (1972). A variable spectral grid spacing is used, selected for any given wavenumber interval considering the proximity and width of the nearest spectral line. A relatively sparse grid with a minimum resolution of 0.1 cm^{-1} was employed in regions of the spectrum where the absorption coefficient was small; higher resolution was used near line centers to ensure at least four points per Doppler or Lorentzian half-width, whichever was smaller. Line widths for pressure broadening were computed according to the expression:

$$\Gamma = \Gamma_0 \left(\frac{P}{P_0}\right)\left(\frac{T_0}{T}\right)^m, \tag{10}$$

where Γ_0 is the line half-width (FWHM) for the appropriate reference values of temperature and pressure, T_0 and P_0, respectively. Doppler widths were obtained using the relation:

$$\gamma = \nu(7\times 10^{-7})\left(\frac{T}{M}\right)^{1/2}, \tag{11}$$

where M is the molecular weight of the absorbing molecule. Contributions from lines within 10 cm^{-1} of a particular spectral point were included explicitly. Profiles for Voigt lines were evaluated using the algorithm presented by Drayson (1976).

The temperature dependence of line strengths was calculated in terms of the appropriate Boltzmann distribution function:

$$S = S_0\left(\frac{Q_0}{Q}\right)\exp\left[-\frac{\mathrm{hc}E}{\mathrm{k}}\left(\frac{T_0-T}{T_0T}\right)\right] \tag{12}$$

where h is Planck's constant; c is the vacuum speed of light; k is Boltzmann's constant; S_0 is the line intensity at the reference temperature, T_0; and E is the energy of the lower state of the transition. The ratio of partition functions, Q_0/Q, is closely approximated by $(T_0/T)^r$, where r equals 1.0 for CO_2, 1.5 for H_2O and O_3. The frequency of individual transitions, together with values for Γ_0 and m in equation (10) and S_0 and E in equation (12), were taken from Rothman *et al.* (1986) for lines in the 15 μ band of CO_2, the 9.6 μ band of O_3 and the 6.3 μ and pure rotation bands of H_2O. We allowed for absorption by all of the relevant isotopic forms of the important infrared active species.

Cumulative probability functions [equation (5)] were computed using a line-by-line analysis with 50 cm^{-1} wide spectral intervals. Results were stored in tabular form and accessed at the beginning of an individual model run. Each table contains 300 $g-k$ pairs, with grid spacings closer near the endpoints in order to represent accurately the head and tail of the probability distribution functions. It was found in practice that fluxes could be obtained to an accuracy of about 1% using a quadrature consisting of about 100 points per 50 cm^{-1} interval. Reduction in the number of quadrature points below this limit was found to introduce significant errors in the stratosphere, reflecting the properties of $g(k)$ at low pressure (cf. Fig. 2b).

Absorption by water vapor in the continuum was taken into account using the parameterization presented by Roberts *et al.* (1976). The effect of overlap between continuum and line absorption can be included only when the humidity profile is specified; we were unable, therefore, to account for continuum absorption in the precomputed cumulative distribution functions. Instead, since the continuum absorption coefficient varies slowly over spectral intervals as small as 50 cm^{-1}, we chose to adjust line absorption optical depths over the course of individual model runs to account for a constant offset associated with the continuum.

As noted by ICRCCM, procedures adopted to carry out the vertical integration in equation (8) are of particular concern. It is appropriate that these issues be addressed in some detail. The problems are associated ultimately with the necessarily finite resolution of models. For models including n levels, temperatures can be determined only for n model locations. We must choose whether to represent the Planck function at the levels used to calculate fluxes, or to employ an average Planck function for included layers. The different approaches are termed the $\tau \mathrm{d}B$ and $B\mathrm{d}\tau$ methods, respectively, by Ridgway *et al.* (1991).

Consider the contribution to the flux at a particular level associated with a layer bounded by levels i and $i+1$. In the $\tau \mathrm{d}B$ method, the flux equation is integrated by parts:

$$\int_i^{i+1} B\,\mathrm{d}E_3 = BE_3\Big|_i^{i+1} - \int_i^{i+1} E_3\,\mathrm{d}B. \tag{13}$$

The second integral is evaluated with assumptions concerning the variation of E_3 and B within the layer $i \rightarrow i+1$ (recall that the temperature can be specified only at the endpoints). Implementing this scheme, we evaluate the mean transmission between the levels by writing:

$$\int_i^{i+1} E_3 \, dB \approx (E_3^{(i)} E_3^{(i+1)})^{1/2} (B^{(i+1)} - B^{(i)}). \quad (14)$$

In contrast, the $B d\tau$ approach assumes an average temperature for the layer. Thus,

$$\int_i^{i+1} B \, dE_3 \approx B_{av}(E_3^{(i+1)} - E_3^{(i)}). \quad (15)$$

The $B d\tau$ option has the disadvantage that the choice for B_{av} is not obvious. The choice of optimum temperature in calculating the flux for the upward direction might be quite inappropriate in computing the flux for the downward direction. The flux emitted by an optically thick layer is expected to reflect the temperature near the layer boundary, rather than the average temperature of the layer. Since the mean optical depth varies significantly for different spectral intervals, it is difficult to identify a single strategy acceptable for all applications.

We chose to address this problem using a higher order quadrature scheme for optically thick layers, defined by $\tau \geqslant 1$, where τ represents the optical thickness of a given layer. For $\tau < 1$ a mean temperature was used to describe the Planck function within the layer. For $\tau \geqslant 1$, the layer was subdivided into smaller units, with an assumption that the Planck function varied linearly with optical depth. (The linear approximation can be shown to be exact for the case of a gray atmosphere.) The layer division can be accomplished using equal increments of optical depth. For $\tau \gg 1$ this would require, however, an inordinately large number of subdivisions. Instead, since the flux integral involves the Planck function weighted by the exponential integral, we chose to subdivide optically thick layers using equal increments of the exponential integral. Fixed divisions of τ were selected to approximate equal incremenets of $E_3(\tau)$ for $\tau = 1$. Specifically, for layers with $\tau \geqslant 1$ the integration was performed using quadrature points at the bounding levels and for optical depths of 0.1τ, 0.3τ and 0.6τ within the layer. The effect for the optically thick case is that the flux originates almost exclusively from the proximate edge of the layer. Average values of the Planck function were used in adjacent layers, together with the linear $B(\tau)$ assumption, to evaluate the Planck function at particular quadrature points. Due to the difference in the approach applied for optically thick layers, we refer to this scheme as the adaptive Bd method.

The vertical integration can be recast in the form o a matrix equation (Curtis, 1956):

$$F_i^{\Delta\nu} = \sum_{j=1}^{n} D_{ij}^{\Delta\nu} B_j^{\Delta\nu}. \quad (16$$

Here, the subscript i refers to a particular model leve while j identifies either the mean layer temperature o the temperatures at the selected (n) levels. The elements of the Curtis matrix, D_{ij}, are determinec according to the previous expressions, with the additional integration over the cumulative distribution function [cf. equation (8)]. The exponentia integral is approximated using either a series expansion for $\Delta\tau < 1.4$, or by continued fractions for $\Delta\tau \geqslant 1.4$. The value of 1.4 was chosen empirically to provide the best compromise between accuracy and computational efficiency; the approach was checked using tabulated values given by Abramowitz and Stegun (1964). Terms were included until results converged to better than one part in 10^4.

To obtain the spectrally integrated flux, equation (16) is summed over all spectral intervals $\Delta\nu_k$, from $k = 1$ to N. Once the Curtis matrix elements are known, equilibrium temperatures are calculated using an iterative Newton–Raphson technique (Coakley, 1977):

$$F_i = \sum_{k=1}^{N} \left[{}^{o}F_i^k + \sum_{j=1}^{n} D_{ij}^k \frac{\partial B_j^k}{\partial T_j} (T_j - {}^{o}T_j) \right], \quad (17)$$

where F_i is the value for the net flux at level i and the superscript (o) refers to results obtained from the previous iteration. The Newton–Raphson method was found to converge in radiative equilibrium calculations, typically after four or five iterations. For applications where the time evolution of the model is not of primary concern, the Newton–Raphson approach is preferable to time-marching approaches which often require 500–1000 time steps to reach equilibrium (e.g. Manabe and Möller, 1961).

Figure 3 compares cooling rates obtained for the mid-latitude summer atmosphere (McClatchey *et al.*, 1972) using the vertical integration schemes discussed above. Also shown are cooling rates calculated using the line-by-line model at the Goddard Laboratory for Atmospheres (Ridgway *et al.*, 1991). Both the adaptive $Bd\tau$ and τdB methods give results in agreement with the line-by-line model to within 10%. The agreement in the latter case is not surprising since the Goddard model employs a vertical integration scheme closely related to τdB; the residual discrepancies may be attributed to differences in the treatment of other

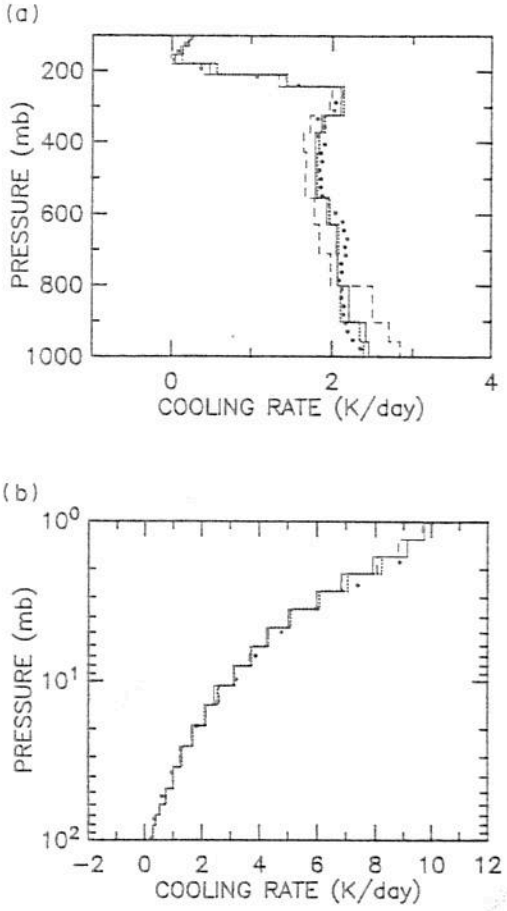

FIG. 3. (a) TROPOSPHERIC COOLING RATES FOR THE MID-LATITUDE SUMMER ATMOSPHERE (MCCLATCHEY *et al.*, 1972). The lines denote cooling rates within model layers according to the τdB (···), $B d\tau$ (- - -), and adaptive $B d\tau$ (——) methods of vertical integration. (●) Cooling rates derived with the line-by-line model at the Goddard Laboratory for Atmospheres (Ridgway *et al.*, 1991). (b) Same as (a), for the stratosphere.

spectral quantities. Cooling rates for $B d\tau$ are 20–30% higher than values obtained with the τdB method near the surface. This arises as a result of errors within optically thick layers. As discussed by Ridgway *et al.* (1991), use of a single temperature for optically thick layers results in a consistent underestimate of the downward flux if the temperature gradient is negative (i.e. for most of the troposphere). Similarly, it results in an overestimate of upward fluxes, except near the surface where the flux is dominated by contributions from the surface itself. The calculated flux divergence is too large for the lower layers and tends to be too small for the mid-troposphere. Ridgway *et al.* (1991) also examined the convergence of results for cooling rates as a function of increasing vertical resolution. They found that the τdB method converged quite rapidly, while the $B d\tau$ approach required considerably higher resolution to achieve comparable accuracy. We conclude that the $B d\tau$ method yields unacceptably large errors. Cooling rates computed for the tropical atmosphere (McClatchey *et al.*, 1972) are compared in Fig. 4. The results demonstrate evident problems with the $B d\tau$ method.

Radiative equilibrium temperatures computed using the τdB and adaptive $B d\tau$ methods are compared in Fig. 5. The calculations summarized here used profiles for H_2O and O_3 appropiate for mid-latitude summer. The upward flux of radiation at the top of the atmosphere was set equal to 265 W m^{-2}. Infrared cooling is balanced in the stratosphere by heating associated with absorption of solar ultraviolet radiation by O_3. Heating rates were computed for diurnally averaged equinoctial conditions at the equator using analytic expressions given by Shimazaki (1985). Heating due to absorption of solar radiation in the near-infrared by water vapor was included in a similar fashion. As indicated, a conspicuous feature

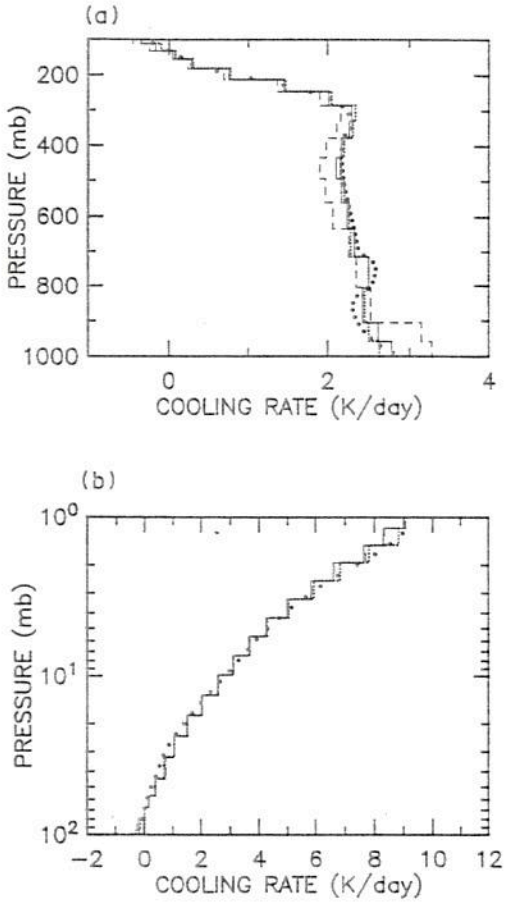

FIG. 4. (a) COOLING RATES COMPUTED FOR THE TROPICAL TROPOSPHERE OF MCCLATCHEY *et al.* (1972). The lines denote cooling rates within model layers according to the τdB (···), $B d\tau$ (- - -), and adaptive $B d\tau$ (——) methods of vertical integration. (●) Line-by-line cooling rates from the Geophysical Fluid Dynamics Laboratory (Luther *et al.*, 1988). (b) Same as (a), for the stratosphere.

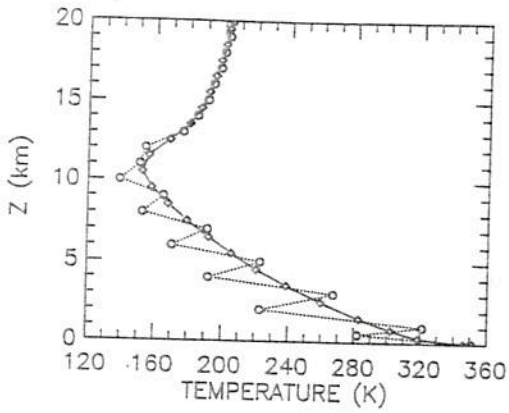

FIG. 5. RADIATIVE EQUILIBRIUM TEMPERATURES CALCULATED WITH τdB (○), AND ADAPTIVE $Bd\tau$ (◇) TECHNIQUES. The emergent flux at the top of the atmosphere is 265 W m^{-2} in both cases. Constitutent profiles are appropriate for the mid-latitude atmosphere in summer.

of the results is the oscillatory behavior observed for level temperatures calculated with the τdB scheme. It arises as a consequence of an over-compensation near fixed temperature boundaries, the surface in this case. The problem could be eliminated by imposing a temperature discontinuity at the surface, although a similar discontinuity would be required also at the top of the convective zone in a fixed lapse rate model. Figure 6, for example, illustrates the temperature profiles that result using a 6.5 K km^{-1} convective adjustment, with absorber profiles and emergent fluxes the same as for Fig. 5. The convective override procedure was implemented in this calculation in the standard fashion (Manabe and Strickler, 1964). The same over-compensation effect is evident in Fig. 6, only in this case the oscillations are driven by the fixed temperature at the upper level of the convectively adjusted region.

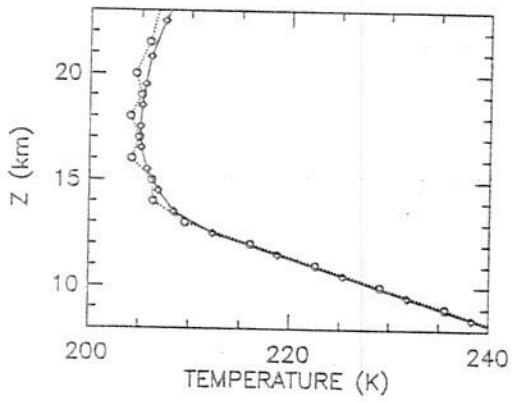

FIG. 6. RADIATIVE–CONVECTIVE EQUILIBRIUM WITH A 6.5 K km^{-1} CONVECTIVE OVERRIDE. (○) Temperatures obtained using the τdB scheme; (◇) temperatures calculated using the adaptive $Bd\tau$ method. Emergent fluxes and constituent profiles are the same as for Fig. 5.

A temperature discontinuity is required to satisfy the boundary conditions, either at the surface or at the top of the convective zone. The temperature jump is well defined for a gray atmosphere. In the case of the present model, the monochromatic flux divergence is not necessarily zero and the magnitude of the temperature discontinuity is not so easily determined. In the real atmosphere, transfer of heat by molecular diffusion and small scale motions would tend to eliminate small-scale temperature variations such as those indicated in Figs 5 and 6. To avoid the difficulty associated with a temperature discontinuity in the model, we chose to carry out the vertical integrations using the adaptive $Bd\tau$ method. The error resulting from the use of this scheme is negligible compared with that for the τdB approach (Figs 3 and 4).

3. CLEAR-SKY FLUXES

We discuss in this section the factors that determine the flux of infrared radiation at the top of the atmosphere. Our strategy is to examine the dependence of the flux on surface temperature for selective changes in model parameters. Model results will be compared with measurements of clear-sky fluxes characterized as a function of sea surface temperature by Raval and Ramanathan (1989). The observations were originally presented in the form of a quantity (G) proposed to represent the greenhouse effect, defined as the difference between the black-body radiation emitted by the sea surface and the emergent flux at the top of the atmosphere. As discussed in Section 1, we find this approach confusing. The energy balance of a cloud-free (non-precipitating) atmospheric column depends not only on the input and output of radiant energy at the surface (E and $F\downarrow_S$, respectively) and on the emission of radiant energy to space ($F\uparrow_T$), but is also affected by exchange of heat by conductive processes at the surface (Q_S), by absorption of solar radiation (S) and by inputs of energy associated with divergence of large scale quasi-horizontal atmospheric motions ($\nabla \cdot H$). The approach here involves separate consideration of $F\uparrow_T$, $F\downarrow_S$ and S, with subsequent evaluation of the remaining terms as residuals in the overall energy balance equation.

As a first step in exploring the factors influencing the magnitude of $F\uparrow_T$, we used a convective adjustment model with the temperature lapse rate set equal to 6.5 K km^{-1} at lower altitudes, where the radiative equilibrium profile was found to be convectively unstable. The mixing ratio of CO_2 was taken as equal to the contemporary value of 350 ppm, with the profile for H_2O selected to agree with observations for summer at mid-latitudes. A climatological mean profile

was adopted for O_3 (Keating and Young, 1985; Dütsch, 1974). Annual mean values of T_s were mapped to appropriate latitudes according to Pickard and Emery (1982). Errors introduced by the mapping are negligible; variations in the profile of O_3 between the equator and 40°N account for only about 4 W m^{-2} of the change inferred for the emergent flux over the corresponding range of surface temperatures.

Figure 7 presents a comparison of calculated fluxes with results derived from ERBE. The agreement is poor, as might be expected given the large changes in the profiles for H_2O expected for the range of surface temperatures included in the figure. The fixed profile for H_2O used in Fig. 7, curve A, results in an atmosphere saturated with respect to H_2O for $T_s = 288$ K, while the model with $T_s = 302$ K is excessively dry, with relative humidity at the surface equal to about 40%. We would have expected better agreement between model and observation for a surface temperature of 294 K, for which the choice of profile for H_2O should be reasonably appropriate. The problem in this case can be traced to the assumption of a fixed (6.5 K km^{-1}) critical lapse rate, as illustrated by the results summarized by curve B. The lapse rate adjustment was treated in a more realistic fashion in this case; we adopted the parameterization suggested by Rennick (1977) which allows an empirical fit to the static stability, $\partial\theta/\partial p$, as a function of T_s. The flux at $T_s = 294$ K for curve B is in excellent agreement with ERBE, while the trend of flux as a function of surface temperature is improved with respect to the model with a constant lapse rate (curve A).

The emergent flux defines an effective temperature identified with an altitude between about 5 and 7 km. Temperatures in this altitude interval are about 2–8 K cooler for the 6.5 K km^{-1} fixed lapse rate model than for the model with the variable parameterized lapse rate. Emergent fluxes are consequently higher in the latter case. Figure 8 shows a comparison of temperature profiles for the two models with a surface temperature of 294 K. The lapse rate parameterization approach, designed to provide results consistent with observed temperatures, produces a lapse rate significantly smaller than 6.5 K km^{-1} in the lower troposphere. Stone and Carlson (1979) have shown that mean tropospheric lapse rates vary significantly with respect to latitude; annual mean values decline from about 6.3 K km^{-1} at the equator to about 5.6 K km^{-1} at 40°N. Rennick's (1977) approach implicitly allows for this variation through the empirical fit of lapse rates to mean surface temperatures. The net effect in our calculations is to reduce the dependence of the emergent flux on surface temperature. This result can be understood by referring to temperatures within the crucial 5–7 km altitude range. In the 6.5 K km^{-1} adjustment model, a difference in surface temperature between two model atmospheres is translated to an identical difference in temperature for any specified altitude in the convective region; the contrast in emergent flux between the $T_s = 288$ and $T_s = 302$ K atmospheres for curve A reflects a 14 K difference in temperature for the 5–7 km altitude region. Lapse rates for the parameterized adjustment model are generally larger for higher values of surface temperature. The contrast in temperatures for the 5–7 km region in curve B is reduced accordingly, to about 9 K over the

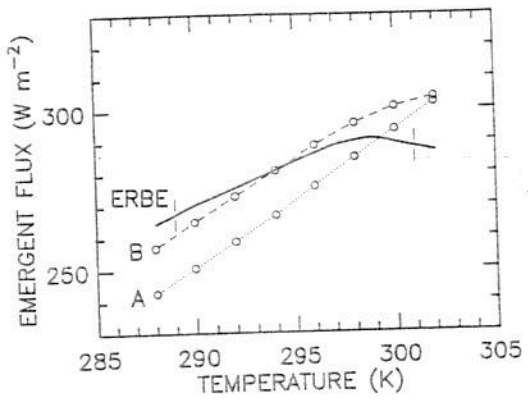

FIG. 7. INFRARED FLUXES AT THE TOP OF THE ATMOSPHERE CALCULATED USING THE 6.5 K km^{-1} ADJUSTMENT MODEL (··· CURVE A), AND THE PARAMETERIZED LAPSE RATE MODEL (--- CURVE B), DISCUSSED IN THE TEXT.
The calculations employ the same atmospheric composition. (——) Annual mean, clear-sky, fluxes measured by ERBE [adapted from Fig. 4 of Raval and Ramanathan (1989)]. The vertical lines indicate the estimated uncertainty in the ERBE data, about 5 W m^{-2}.

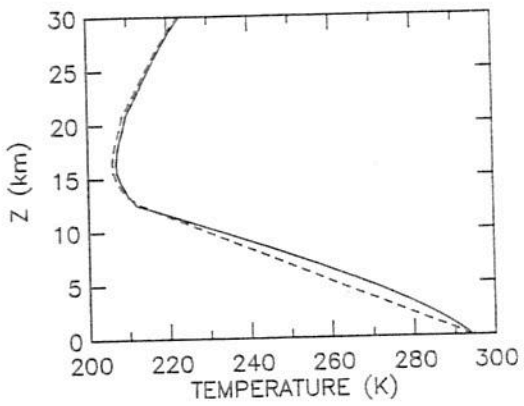

FIG. 8. COMPARISON OF MODEL TEMPERATURES OBTAINED WITH THE 6.5 K km^{-1} ADJUSTMENT MODEL (---) AND THE PARAMETERIZED LAPSE RATE MODEL (——).
Composition and surface temperature are identical in both models. Temperatures in the middle troposphere are about 6 K cooler for the 6.5 K km^{-1} model as compared with the parameterized lapse rate model.

range $T_s = 288$–302 K; the gradient in emergent flux as a function of surface temperature is correspondingly diminished. The 6.5 K km^{-1} lapse rate adjustment model is inadequate, not only in simulating the variation of emergent flux with latitude, but also in describing the global average value of the emission to space.

The agreement between model and ERBE data can be improved by use of a fixed profile for relative humidity as a function of pressure as indicated in Fig. 9. The fluxes represented by curve C were obtained with a simulation of H_2O consistent with the relative humidity profile introduced by Manabe and Wetherald (1967):

$$RH(p) = RH(p_0)\left[\frac{p}{p_0}\right], \tag{18}$$

where RH is the relative humidity, p is the pressure, and p_0 is the pressure at the surface. Equation (18) predicts mixing ratios for H_2O in the upper troposphere and stratosphere which frequently fall below 4.5 ppmv, the value adopted for the average value of the mixing ratio of H_2O in the stratosphere. We chose, therefore, to truncate the expression for $RH(p)$ given by equation (18) at the level where the mixing ratio of H_2O declined to 4.5 ppmv; the mixing ratio of H_2O was assumed constant, equal to 4.5 ppmv, at higher levels. The surface humidity was set equal to 80% for the entire range of T_s. Relative humidities were referenced to saturation pressures over water using the expression given by List (1958). Specific humidities adopted by the model for the region from the surface to 500 mbar are broadly consistent with zonal mean humidities reported by Oort and Rasmussen (1971) and Newell *et al.* (1972). Values for the column abundance of water vapor implied by the model are also in good agreement with microwave measurements presented as functions of sea surface temperature by Stephens (1990).

The results summarized by curve C in Fig. 9 were obtained with a 6.5 K km^{-1} constant adjustment for the lapse rate in the convectively unstable region. A variable lapse rate, in combination with variable H_2O, provides excellent agreement with ERBE data for surface temperatures less than 298 K, as shown in Fig. 10. The emergent flux predicted by the model is higher than the observed value by 4.4 W m^{-2} for a surface temperature of 300 K; the discrepancy grows to about 10 W m^{-2} for a temperature of 302 K. Recognizing that relative humidities over the warmest regions of the ocean may be as high as 85%, we repeated the calculations with surface relative humidities adjusted to this larger value. The value for the emergent flux at 302 K was reduced by only 1.6 W m^{-2}, indicating that the emergent flux is not particularly sensitive to a uniform change in the profile for relative humidity. Emergent fluxes are sensitive, however, to values assumed for the abundance of H_2O in the middle and upper troposphere. Figure 10 illustrates the effect of imposing minimum values of 35% and 50% for relative humidities corresponding to the $T_s = 300$ and 302 K cases, respectively. In these simulations, relative humidities were set equal to the specified minimum values for altitudes where values of relative humidity predicted by equation (18) would otherwise have dropped below the assumed minimum. Mixing ratios of H_2O in the stratosphere were fixed as before equal to 4.5 ppmv. The increase in mixing ratios of H_2O between 500 mbar and the tropopause, as much as a factor of 2 in the extreme case, was sufficient to reduce

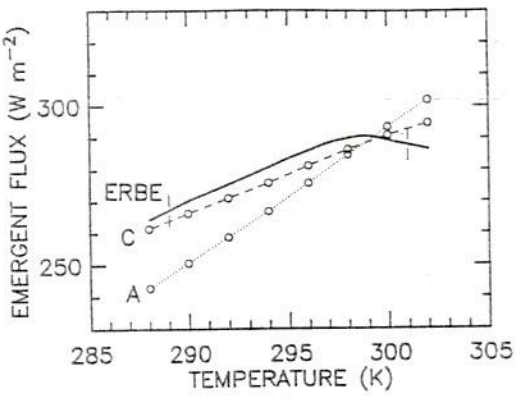

FIG. 9. SAME AS FIG. 7, EXCEPT THAT THE DASHED CURVE (---) REPRESENTS FLUXES OBTAINED WITH THE 6.5 K km^{-1} ADJUSTMENT MODEL USING A FIXED PROFILE FOR RELATIVE HUMIDITY.

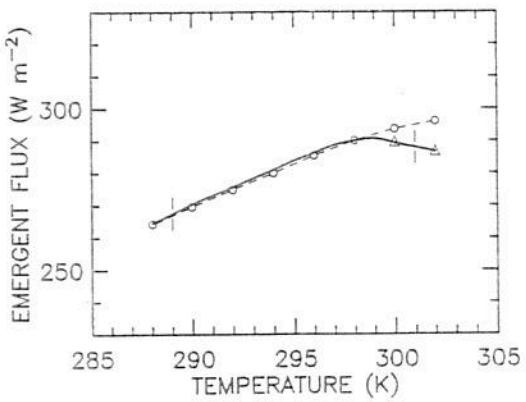

FIG. 10. EMERGENT FLUXES AS CALCULATED USING THE PARAMETERIZED LAPSE RATE MODEL WITH A FIXED PROFILE FOR RELATIVE HUMIDITY (---).

(△) Fluxes obtained for higher concentrations of H_2O in the middle and upper troposphere, as discussed in the text. As for Figs 7 and 9, the solid line (——) refers to the fluxes measured by ERBE.

the emergent flux, allowing excellent agreement with observation as indicated in Fig. 10.

The reduction in emergent flux for $T_s > 298$ K is related to the super greenhouse effect discussed by Raval and Ramanathan (1989). The results presented here suggest that the phenomenon is due, most probably, to a moistening of the middle and upper troposphere over the warmest regions of the ocean in excess of that predicted on the basis of an assumed latitudinally fixed profile for relative humidity. Since the warmer sea surface temperatures are usually accompanied by vigorous convection, particularly in the Western Pacific (Ramage, 1968), a plausible mechanism for moistening involves detrainment and re-evaporation of liquid water and ice from convective towers, as discussed for example by Rind *et al.* (1991). There is no independent means to confirm this possibility, since humidities inferred from radiosonde measurements for the tropics above 500 mbar are fraught with uncertainty (Newell *et al.*, 1972). Mastenbrook (1968) reported a limited set of accurate humidity profiles for Trinidad, West Indies (11°N). His results are compared with the $T_s = 300$ K, 35% minimum relative humidity model in Fig. 11. The annual mean sea surface temperature in this region of the Caribbean is nearly 300 K. Also shown in Fig. 10 are results for annual mean humidities reported by Oort and Rasmusson (1971) for 10°N. The increase in humidity invoked by the model with respect to the reference profile of equation (18) is consistent with existing measurements, at least for the case $T_s = 300$ K.

We turn our attention now to implications of the model for the downward flux of infrared radiation at the surface, the quantity most directly related to the greenhouse effect. In the absence of back-radiation from the atmosphere, the temperature of the surface would assume a global average value of about 253 K, some 35 K cooler than the value observed. Fluxes of downward infrared radiation at the surface calculated using the constant relative humidity, parameterized lapse rate model are presented in Fig. 12. The calculations for surface temperatures of 300 and 302 K allowed for moistening of the middle and upper troposphere as included in Fig. 10. As illustrated, the variation of the downward flux is nearly linear as a function of surface temperature; the super greenhouse phenomenon observed for the emergent flux has no detectable influence on $F\downarrow_S$. The magnitude of the downward flux defines an effective radiating temperature associated typically with the 2–4 km region of the atmosphere. We conclude that the infrared flux reaching the surface is sensitive primarily to the composition and temperature of the atmosphere between the surface and about 4 km. Additional water vapor postulated for the atmosphere above 5 km at warmer surface temperatures has little effect on the flux of infrared radiation reaching the surface.

4. RADIATIVE FORCING

The net deficit in radiative energy for the clear-sky atmosphere may be computed as a residual according to the relation:

$$R = F\uparrow_T + F\downarrow_S - E - S, \tag{19}$$

where $F\uparrow_T$ is the net upward flux at the top of the

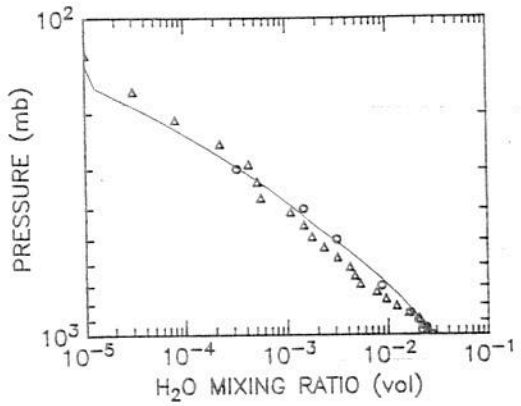

FIG. 11. MIXING RATIOS FOR WATER VAPOR IN THE $T_S = 300$ K ATMOSPHERE WITH 35% MINIMUM RELATIVE HUMIDITY (SOLID). (△) Mean of 25 soundings taken by Mastenbrook (1968) from Trinidad, West Indies (11°N). Circles (○) are annual and zonal mean data for 10°N from Oort and Rasmusson (1971).

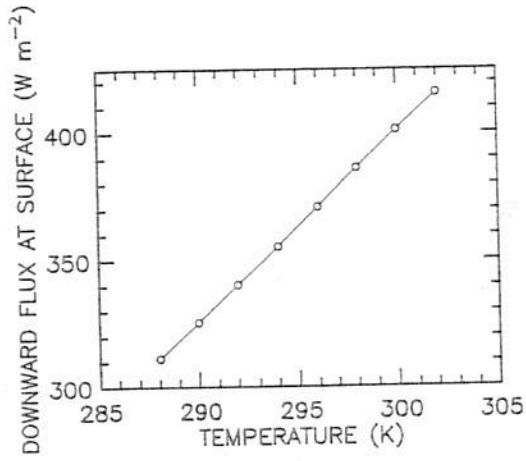

FIG. 12. DOWNWARD FLUXES OF INFRARED RADIATION AT THE SURFACE COMPUTED USING THE PARAMETERIZED LAPSE RATE MODEL WITH A FIXED PROFILE FOR RELATIVE HUMIDITY. The model allows for enhanced concentrations of H_2O in the mid to upper troposphere for surface temperatures of 300 and 302 K, as discussed in the text.

atmosphere, $F\downarrow_S$ is the downward flux at the surface, E is the input of infrared radiation to the atmosphere from the surface and S defines the net absorption of solar radiation by the atmosphere. With our assumptions, absorption of solar radiation in the stratosphere is balanced by net emission of infrared radiation—the stratosphere is in radiative equilibrium. It follows that the magnitude of the radiative deficit for the troposphere is precisely the same as for the atmosphere as a whole; the net upward flux of infrared radiation at the tropopause is less than the flux at the top of the atmosphere by an amount precisely equal to the flux of solar radiation absorbed by the stratosphere. Components of the radiant energy budget of the atmosphere, together with the residual or radiative deficit, are presented as functions of surface temperature for the cloud-free environment in Fig. 13. Note that, with our definition for R, a positive deficit implies a net loss of radiant energy which must be balanced by a source of heat supplied by atmospheric motion.

The results in Fig. 13 indicate that interactions with the radiation field involve a net loss of energy by the clear atmosphere, a deficit of between 120 and 150 W m^{-2} for the range of surface temperatures considered here. For time scales longer than the time for radiative relaxation (about 25 days), this deficit must be balanced by an influx of energy to the vertical column. The energy budget for a vertical column of clear atmosphere in steady state satisfies the equation:

$$F\uparrow_T + F\downarrow_S - E - S - Q_S + \nabla \cdot H = 0, \qquad (20)$$

where Q_S is the upward flux of sensible heat supplied to the atmosphere by the surface. The average value of Q_S over the ocean is comparatively small, ranging from about 15 W m^{-2} at the equator to 30 W m^{-2} at mid-latitudes (Sellers, 1965). The last term in equation (20) allows for the transport of dry static energy out of the atmospheric column,

$$H = \int V(c_p T + \Phi)\, dp, \qquad (21)$$

where V is the horizontal wind velocity, and $\Phi = gz$ is the geopotential energy. The balance represented by equation (20) omits the contribution associated with transport of kinetic energy, which is negligible compared with that for dry static energy described by equation (21) (e.g. Oort and Rasmusson, 1971).

Since Q_S is small, the clear-sky radiative deficit must be compensated primarily by convergence of dry static energy. Horizontal temperature gradients are small over the tropical and subtropical oceans, loosely identified here with a range of surface temperatures from about 296 to 302 K, and H is dominated by the flux of geopotential energy: the clear-sky radiative deficit is balanced by heating associated with subsidence caused by convergence of air aloft, as discussed for example by Gray (1973) and Yanai *et al.* (1973). The geopotential flux is ultimately supplied by upward motion in cumulus towers in the region of the equatorial trough (Riehl and Malkus, 1958). As pointed out by Gray (1973), latent heat released in cumulus clouds is used to drive upward motion. Energy is exported to the surrounding environment in the form of potential energy which is realized eventually as heat released as a result of compensatory subsidence. The clear-sky radiative deficit, as indicated in Fig. 14, is almost constant over the temperature range 298–302 K. The trend exhibited here

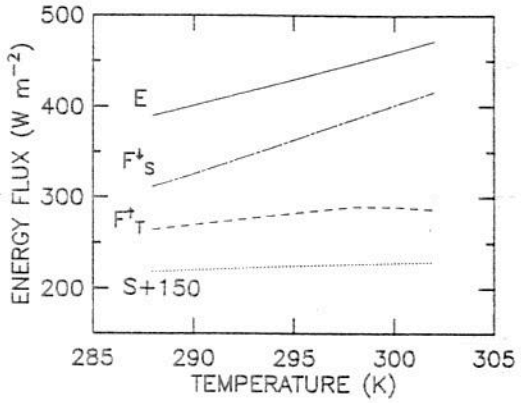

FIG. 13. COMPONENTS OF THE RADIATIVE ENERGY BUDGET OF THE ATMOSPHERE.
E describes the input of infrared radiation at the surface; $F\uparrow_T$ is the emergent flux at the top of the atmosphere; $F\downarrow_S$ is the downward flux at the surface; and S represents the height integrated absorption of solar radiation (note that 150 W m^{-2} has been added to S for clarity of presentation).

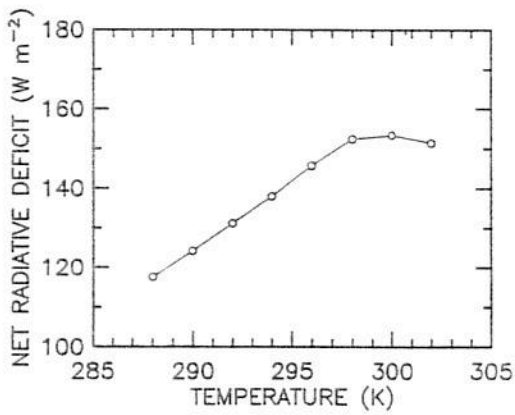

FIG. 14. NET RADIATIVE DEFICIT OF THE TROPOSPHERE CORRESPONDING TO THE FLUXES SUMMARIZED IN FIG. 13.
The analysis allows for enhanced concentrations of H_2O at upper levels of the troposphere for surface temperatures higher than 298 K, as discussed in the text.

is related ultimately to the behavior of the emergent flux at high T_s, the super greenhouse phenomenon discussed by Raval and Ramanathan (1989). The implication is that rates of clear-sky subsidence are relatively constant in the tropics, independent of T_s. Allowing for a contribution of 15 W m^{-2} for Q_S, we estimate that an energy balance can be maintained for a range of sea surface temperatures from about 296 to 302 K with a mean downward mass flux of 25–30 mbar day^{-1}. A flux of this magnitude is in agreement with observations for the western tropical Pacific (Balsley *et al.*, 1988), which indicate clear-sky sinking motions of 15–40 mbar day^{-1}. Our results are consistent with simple models of the tropical energy budget as presented, for example, by Sarachik (1978).

5. SUMMARY AND CONCLUSION

A computationally efficient radiative model has been developed and shown to provide an accurate representation of radiative cooling rates and infrared radiative fluxes. The model was applied to analysis of the ERBE data for clear-sky conditions.

The flux of infrared radiation emitted to space was shown to be sensitive to lapse rates assumed for temperatures in the lower troposphere and to the abundance of H_2O in the middle troposphere, specifically to conditions in the 5–7 km altitude region. The ERBE data indicate an increase in emergent fluxes as a function of surface temperature for temperatures in the range 288–298 K. This behavior is accurately reproduced by a radiative–convective model characterized by a constant profile for relative humidity as a function of pressure, with lapse rates for temperature specified in the lowest regions of the atmosphere on the basis of the empirical relationship presented by Rennick (1977). The ERBE data suggest a small decrease in emergent fluxes for surface temperatures above 298 K; this phenomenon, termed the super greenhouse by Raval and Ramanathan (1989), is associated with an increase in the abundance of H_2O in the middle and upper troposphere with respect to the constant relative humidity profile adopted as standard for the simulations at lower temperatures. The moistening at warmer surface temperatures is attributed to enhanced convective activity, with water supplied in both vapor and condensed phases to upper levels of the troposphere.

Greenhouse forcing at the surface is relatively insensitive to the additional burden of H_2O vapor inferred for the middle and upper troposphere when surface temperatures exceed about 298 K. The flux of infrared radiation from the atmosphere to the surface is determined largely by conditions in the bottom 4 km of the atmosphere. It is regulated primarily by the gradient of temperature near the surface and by the abundance and distribution of H_2O at the lowest altitudes. The latter is controlled mainly by surface temperature and is simulated adequately by the latitudinally independent profile adopted as reference for the variation of relative humidity with pressure. A decrease in the temperature of the levels radiating to space in the tropics, due largely to a higher burden of H_2O in the middle and upper troposphere, compensates for reduced net heating of the atmosphere by the surface in the warmer, moister, environment of the lower atmosphere in this region; the quantity $E-F\downarrow_S$, as indicated in Fig. 13, is predicted to decrease as a function of increasing surface temperature. The clear-sky radiative deficit of the atmosphere in the tropics and sub-tropics is relatively constant and is balanced by heat released due to subsidence at a rate of about 25–30 mbar day^{-1}.

The analysis implies a relatively simple picture for the mean energy budget of the clear-sky troposphere at low latitudes. Localized convection during the day in warmer regions adds moisture to the upper troposphere. Radiative cooling is balanced by sinking motion in cloud free environments with associated release of geopotential energy. It should be emphasized that the feedbacks identified in this study and the inferences drawn with respect to specific variations of the abundance and distribution of tropospheric H_2O as a function of surface temperature are defined only for the present climate. Extensions to other environments, higher levels of CO_2 for example, will require a more comprehensive physical model for climate. The analysis described here can provide valuable constraints in the development and validation of such a model.

Acknowledgements—This work was supported by National Science Foundation grant ATM-89-21119 to Harvard University; K. Minschwaner also wishes to thank the Alexander Host Foundation for fellowship support. We are grateful to W. L. Ridgway for making available results of line-by-line calculations. We acknowledge instructive conversations with Richard M. Goody.

REFERENCES

Abramowitz, M. and Stegun, I. A. (1964) *Handbook of Mathematical Functions*. Applied Mathematics Series, Vol. 55, National Bureau of Standards, Washington, D.C.

Arking, A. and Grossman, K. (1972) The influence of line shape and band structure on temperatures in planetary atmospheres. *J. atmos. Sci.* **29**, 937.

Balsley, B. B., Ecklund, W. L., Carter, D. A., Riddle, A. C. and Gage, K. S. (1988) Average vertical motions in the tropical atmosphere observed by a radar wind profiler on

Pohnpei (7°N latitude, 157°E longitude). *J. atmos. Sci.* **45**, 396.
Barkstrom, B. R. (1984) The Earth Radiation Budget Experiment (ERBE). *Bull. Am. Met. Soc.* **65**, 1170.
Coakley, J. A. Jr (1977) An efficient numerical approach to radiative–convective equilibrium. *J. atmos. Sci.* **34**, 1402.
Curtis, A. R. (1956) The computation of radiative heating rates in the atmosphere. *Proc. R. Soc. A* **236**, 156.
Drayson, S. R. (1976) Rapid computation of the Voigt profile. *J. quant. Spectrosc. radiat. Transfer* **16**, 611.
Dütsch, H. U. (1974) The ozone distribution in the atmosphere. *Can. J. Chem.* **52**, 1491.
Ellingson, R. G., Ellis, J. and Fels, S. (1991) The intercomparison of radiation codes used in climate models: long wave results. *J. geophys. Res.* **96**, 8929.
Ellsaesser, H. W. (1984) The climatic effect of CO_2: a different view. *Atmos. Environ.* **18**, 431.
Fang, T.-M., Wofsy, S. C. and Dalgarno, A. (1974) Opacity distribution functions and absorption in Schumann–Runge bands of molecular oxygen. *Planet. Space Sci.* **22**, 413.
Fels, S. B., Kiehl, J. T., Lacis, A. A. and Schwarzkopf, M. D. (1991) Infrared cooling rate calculations in operational general circulation models: comparison with benchmark calculations. *J. geophys. Res.* **96**, 9105.
Goody, R. M., West, R., Chen, L. and Crisp, D. (1989) The correlated-*k* method for radiation calculations in nonhomogeneous atmospheres. *J. quant. Spectrosc. radiat. Transfer* **42**, 539.
Goody, R. M. and Yung, Y. L. (1989) *Atmospheric Radiation: Theoretical Basis*, 2nd edn. Oxford University Press, New York.
Gray, W. M. (1973) Cumulus convection and larger scale circulations I. Broadscale and mesoscale considerations. *Mon. Weath. Rev.* **101**, 839.
Hansen, J., Johnson, D., Lacis, A., Lebedeff, S., Lee, P., Rind, D. and Russell, G. (1981) Climatic impact of increasing carbon dioxide. *Science* **213**, 957.
Hansen, J., Russell, G., Rind, D., Stone, P., Lacis, A., Lebedeff, S., Ruedy, R. and Travis, L. (1983) Efficient three-dimensional global models for climate studies: models I and II. *Mon. Weath. Rev.* **111**, 609.
Keating, G. M. and Young, D. F. (1985) Interim reference ozone models for the middle atmosphere. In *Handbook for MAP*, Vol. 16 (Edited by Labitzke, K., Barnett, J. J. and Edwards, B.), pp. 205–229. SCOSTEP Secretariat, University of Illinois, Urbana, IL.
Lacis, A. A. and Oinas, V. (1991) A description of the correlated-*k* distribution method for modeling nongray gaseous absorption, thermal emission, and multiple scattering in vertically inhomogeneous atmospheres. *J. geophys. Res.* **96**, 9027.
Lindzen, R. S. (1990) Some coolness concerning global warming. *Bull. Am. Met. Soc.* **71**, 288.
List, R. J., Ed. (1958) *Smithsonian Meteorological Tables*. Washington, D.C.
Luther, F. M., Ellingson, R. G., Fouquart, Y., Fels, S. B., Scott, N. and Wiscombe, W. J. (1988) Intercomparison of radiation codes in climate models (ICRCCM): longwave clear-sky results—a workshop summary. *Bull. Am. Met. Soc.* **69**, 40.
Manabe, S. and Möller, F. (1961) On the radiative equilibrium and heat balance of the atmosphere. *Mon. Weath. Rev.* **89**, 503.
Manabe, S. and Strickler, R. F. (1964) Thermal equilibrium of the atmosphere with a convective adjustment. *J. atmos. Sci.* **21**, 361.
Manabe, S. and Wetherald, R. T. (1967) Thermal equilibrium of the atmosphere with a given distribution of relative humidity. *J. atmos. Sci.* **24**, 241.
Mastenbrook, H. J. (1968) Water vapor distribution in the stratosphere and high troposphere. *J. atmos. Sci.* **25**, 299.
McClatchey, R. A., Fenn, R. W., Selby, J. E. A., Volz, F. E. and Garing, J. S. (1972) Optical properties of the atmosphere. *Environ. Res. Pap. 411*, 108 pp. Air Force Cambridge Research Laboratory, Bedford, MA.
Newell, R. E., Kidson, J. W., Vincent, D. G. and Boer, G. J. (1972) *The General Circulation of the Tropical Atmosphere*, Vol. 1. MIT Press, Cambridge, MA.
Oort, A. H. and Rasmusson, E. M. (1971) Atmospheric circulation statistics. *NOAA Proc.*, paper 5.
Pickard, G. L. and Emery, W. J. (1982) *Descriptive Physical Oceanography*, 4th edn. Pergamon Press, Oxford.
Ramage, C. S. (1968) Role of a tropical "maritime continent" at atmospheric circulation. *Mon. Weath. Rev.* **96**, 365.
Ramanathan, V. (1976) Radiative transfer within the Earth's troposphere and stratosphere: a simplified radiative–convective model. *J. atmos. Sci.* **33**, 1330.
Raval, A. and Ramanathan, V. (1989) Observational determination of the greenhouse effect. *Science* **342**, 758.
Rennick, M. A. (1977) The parameterization of tropospheric lapse rates in terms of surface temperatures. *J. atmos. Sci.* **34**, 854.
Ridgway, W. L., Harshvardhan and Arking, A. (1991) Computation of atmospheric cooling rates by exact and approximate methods. *J. geophys. Res.* **96**, 8969.
Riehl, H. and Malkus, J. S. (1958) On the heat balance of the equatorial trough zone. *Geophysica* **6**, 503.
Rind, D., Chiou, E. W., Chu, W., Larson, J., Oltmans, S., Lerner, J., McCormick, M. P. and McMaster, L. (1991) Positive water vapor feedback in climate models confirmed by satellite data. *Nature, Lond.* **349**, 500.
Roberts, R. E., Selby, J. E. A. and Biberman, L. M. (1976) Infrared continuum absorption by atmospheric water vapor in the 8–12 μ window. *Appl. Opt.* **15**, 2085.
Rothman, L. S., Gamache, R. R., Goldman, A., Brown, L. R., Toth, R. A., Pickett, H. M., Poynter, R. L., Fland, J. M., Camy-Peyret, C., Barbe, A., Husson, N., Rinsland, C. P. and Smith, M. A. (1986) HITRAN database: 1986 edition. *Appl. Opt.* **26**, 4058.
Sarachik, E. S. (1978) Tropical sea surface temperature: an interactive one-dimensional atmosphere ocean model. *Dyn. Atmos. Oceans* **2**, 455.
Sellers, W. D. (1965) *Physical Climatology*. University of Chicago Press, Chicago, IL.
Shimazaki, T. (1985) *Minor Constituents in the Middle Atmosphere*. Terra Scientific, Tokyo, Japan.
Stephens, G. L. (1990) On the relationship between water vapor over the oceans and sea surface temperature. *J. Climate* **3**, 634.
Stone, P. H. and Carlson, J. H. (1979) Atmospheric lapse rate regimes and their parameterization. *J. atmos. Sci.* **36**, 415.
Vardavas, I. M. and Carver, J. H. (1984) Solar and terrestrial parameterizations for radiative–convective models. *Planet. Space Sci.* **32**, 1307.
Yanai, M., Esbensen, S. and Chu, J. (1973) Determination of bulk properties of tropical cloud clusters from large-scale heat and moisture budgets. *J. atmos. Sci.* **30**, 611.